

## ENGINEERING

## Confinement, chaotic transport, and trapping of active swimmers in time-periodic flows

Boyang Qin<sup>1,2\*</sup> and Paulo E. Arratia<sup>3\*</sup>

Microorganisms encounter complex unsteady flows, including algal blooms in marine settings, microbial infections in airways, and bioreactors for vaccine and biofuel production. Here, we study the transport of active swimmers in two-dimensional time-periodic flows using Langevin simulations and experiments with swimming bacteria. We find that long-term swimmer transport is controlled by two parameters, the pathlength of the unsteady flow and the normalized swimmer speed. The pathlength nonmonotonically controls swimmer dispersion dynamics, giving rise to three distinct dispersion regimes. Weak flows hinder swimmer transport by confining cells toward flow manifolds. As pathlength increases, chaotic transport along flow manifolds initiates, maximizing the number of unique flow cells traveled. Last, strong flows trap swimmers at the vortex core, suppressing dispersal. Experiments with *Vibrio cholerae* showed qualitative agreement with model dispersion patterns. Our results reveal that nontrivial chaotic transport can arise in simple unsteady flows and suggest a potentially optimal dispersal strategy for microswimmers in nature.

## INTRODUCTION

For algal blooms, a sea-level rise, or a sea-level fall, active swimmers in two-dimensional time-periodic flows are affected by the flow's unsteady dynamics. Large oceanic flows such as the equatorial oceanic gyres, the North Atlantic gyre, and the North Pacific gyre are characterized by their complex unsteady flows (1–3). As a result, these flows are characterized by their complex unsteady dynamics, giving rise to three distinct dispersion regimes. Weak flows hinder swimmer transport by confining cells toward flow manifolds. As pathlength increases, chaotic transport along flow manifolds initiates, maximizing the number of unique flow cells traveled. Last, strong flows trap swimmers at the vortex core, suppressing dispersal. Experiments with *Vibrio cholerae* showed qualitative agreement with model dispersion patterns. Our results reveal that nontrivial chaotic transport can arise in simple unsteady flows and suggest a potentially optimal dispersal strategy for microswimmers in nature.

Microorganisms encounter complex unsteady flows, including algal blooms in marine settings, microbial infections in airways, and bioreactors for vaccine and biofuel production. Here, we study the transport of active swimmers in two-dimensional time-periodic flows using Langevin simulations and experiments with swimming bacteria. We find that long-term swimmer transport is controlled by two parameters, the pathlength of the unsteady flow and the normalized swimmer speed. The pathlength nonmonotonically controls swimmer dispersion dynamics, giving rise to three distinct dispersion regimes. Weak flows hinder swimmer transport by confining cells toward flow manifolds. As pathlength increases, chaotic transport along flow manifolds initiates, maximizing the number of unique flow cells traveled. Last, strong flows trap swimmers at the vortex core, suppressing dispersal. Experiments with *Vibrio cholerae* showed qualitative agreement with model dispersion patterns. Our results reveal that nontrivial chaotic transport can arise in simple unsteady flows and suggest a potentially optimal dispersal strategy for microswimmers in nature.

Even in steady flows, a flow's unsteady dynamics can affect the transport of active swimmers. For example, in a steady flow, a swimmer's trajectory is confined to a manifold. In an unsteady flow, a swimmer's trajectory can be chaotic, allowing it to explore a larger volume of the flow. This chaotic transport is characterized by its nonmonotonic dependence on the flow's pathlength. Weak flows hinder swimmer transport by confining cells toward flow manifolds. As pathlength increases, chaotic transport along flow manifolds initiates, maximizing the number of unique flow cells traveled. Last, strong flows trap swimmers at the vortex core, suppressing dispersal. Experiments with *Vibrio cholerae* showed qualitative agreement with model dispersion patterns. Our results reveal that nontrivial chaotic transport can arise in simple unsteady flows and suggest a potentially optimal dispersal strategy for microswimmers in nature.

<sup>1</sup>Department of Mechanical and Aerospace Engineering, Princeton University, Princeton, NJ 08544, USA. <sup>2</sup>Department of Molecular Biology, Princeton University, Princeton, NJ 08544, USA. <sup>3</sup>Department of Mechanical Engineering and Applied Mechanics, University of Pennsylvania, Philadelphia, PA 19104, USA.

\*Corresponding author. Email: bqin@princeton.edu (B.Q.); parratia@seas.upenn.edu (P.E.A.)

confinement, chaotic transport, and trapping of active swimmers in time-periodic flows. We find that long-term swimmer transport is controlled by two parameters, the pathlength of the unsteady flow and the normalized swimmer speed. The pathlength nonmonotonically controls swimmer dispersion dynamics, giving rise to three distinct dispersion regimes. Weak flows hinder swimmer transport by confining cells toward flow manifolds. As pathlength increases, chaotic transport along flow manifolds initiates, maximizing the number of unique flow cells traveled. Last, strong flows trap swimmers at the vortex core, suppressing dispersal. Experiments with *Vibrio cholerae* showed qualitative agreement with model dispersion patterns. Our results reveal that nontrivial chaotic transport can arise in simple unsteady flows and suggest a potentially optimal dispersal strategy for microswimmers in nature.

In steady flows, a swimmer's trajectory is confined to a manifold. In an unsteady flow, a swimmer's trajectory can be chaotic, allowing it to explore a larger volume of the flow. This chaotic transport is characterized by its nonmonotonic dependence on the flow's pathlength. Weak flows hinder swimmer transport by confining cells toward flow manifolds. As pathlength increases, chaotic transport along flow manifolds initiates, maximizing the number of unique flow cells traveled. Last, strong flows trap swimmers at the vortex core, suppressing dispersal. Experiments with *Vibrio cholerae* showed qualitative agreement with model dispersion patterns. Our results reveal that nontrivial chaotic transport can arise in simple unsteady flows and suggest a potentially optimal dispersal strategy for microswimmers in nature.

voices. As a  $\epsilon$  increases, we observe a decrease in flow velocity as a function of flow path length. They differ by a factor of  $\sqrt{2}$  from the theoretical prediction by the swimming velocity  $U_s$ . We observe a decrease in flow velocity as a function of flow path length. They differ by a factor of  $\sqrt{2}$  from the theoretical prediction by the swimming velocity  $U_s$ . We observe a decrease in flow velocity as a function of flow path length. They differ by a factor of  $\sqrt{2}$  from the theoretical prediction by the swimming velocity  $U_s$ .

Experiments show that the flow velocity is independent of the flow path length. This is consistent with the theoretical prediction. We observe a decrease in flow velocity as a function of flow path length. They differ by a factor of  $\sqrt{2}$  from the theoretical prediction by the swimming velocity  $U_s$ . We observe a decrease in flow velocity as a function of flow path length. They differ by a factor of  $\sqrt{2}$  from the theoretical prediction by the swimming velocity  $U_s$ .

The flow velocity is independent of the flow path length. This is consistent with the theoretical prediction. We observe a decrease in flow velocity as a function of flow path length. They differ by a factor of  $\sqrt{2}$  from the theoretical prediction by the swimming velocity  $U_s$ . We observe a decrease in flow velocity as a function of flow path length. They differ by a factor of  $\sqrt{2}$  from the theoretical prediction by the swimming velocity  $U_s$ .

over the velocity  $U_s$ . The flow velocity is independent of the flow path length. This is consistent with the theoretical prediction. We observe a decrease in flow velocity as a function of flow path length. They differ by a factor of  $\sqrt{2}$  from the theoretical prediction by the swimming velocity  $U_s$ . We observe a decrease in flow velocity as a function of flow path length. They differ by a factor of  $\sqrt{2}$  from the theoretical prediction by the swimming velocity  $U_s$ .

## RESULTS

### Emergence of distinct swimmer transport patterns is universally controlled by the flow pathlength

We observed the emergence of distinct swimmer transport patterns in *Vibrio cholerae* swimming in a channel. The flow velocity is independent of the flow path length. This is consistent with the theoretical prediction. We observe a decrease in flow velocity as a function of flow path length. They differ by a factor of  $\sqrt{2}$  from the theoretical prediction by the swimming velocity  $U_s$ . We observe a decrease in flow velocity as a function of flow path length. They differ by a factor of  $\sqrt{2}$  from the theoretical prediction by the swimming velocity  $U_s$ .

To understand the emergence of distinct swimmer transport patterns, we conducted a series of experiments. The flow velocity is independent of the flow path length. This is consistent with the theoretical prediction. We observe a decrease in flow velocity as a function of flow path length. They differ by a factor of  $\sqrt{2}$  from the theoretical prediction by the swimming velocity  $U_s$ . We observe a decrease in flow velocity as a function of flow path length. They differ by a factor of  $\sqrt{2}$  from the theoretical prediction by the swimming velocity  $U_s$ .

**Flow pathlength nonmonotonically controls four swimmer dispersion regimes**

As the flow pathlength  $p$  increases, we find a sequence of active swimmer dispersion regimes. For low flow frequencies ( $p < 0.5$ ), the swimmers behave as "free swimmers." The stochastic SD scales as  $MSD/l^2$  for  $p < 0.5$  (Fig. 1F), and the SD scales as  $MSD/l^2$  for  $p < 0.5$  (Fig. 1G). However, we observe a transition to a different SD regime by a factor of  $1/2$  (Fig. 1F). Collectively, the stochastic SD scales as  $MSD/l^2$  for  $p < 0.5$  (Fig. 1F). We call this a "vortex trapping regime." The transition of these stochastic regimes occurs for a range of swimmers as a function of  $p$  (Fig. 1G). These results are a consequence of the flow frequency  $f$  and the pathlength  $p$  of the flow. The sequence of flow frequencies  $f$  and pathlengths  $p$  is shown in Fig. 2A-D.

exponent  $n$  increases from  $1.0$  (regime I, Fig. 1G), characteristic of free diffusion, to  $2.0$  (regime II, Fig. 1G), characteristic of ballistic transport. We call this a "manifold trafficking regime." For  $p > 5$ , the swimmers exhibit a different SD regime, which we call a "vortex trapping regime." The transition of these stochastic regimes occurs for a range of swimmers as a function of  $p$  (Fig. 1G). These results are a consequence of the flow frequency  $f$  and the pathlength  $p$  of the flow. The sequence of flow frequencies  $f$  and pathlengths  $p$  is shown in Fig. 2A-D.

**Distinct dispersion patterns underlie different swimmer transport regimes**

Next, we examine the dispersion patterns of the swimmers in the different regimes. The results are shown in Fig. 2A-D. The sequence of flow frequencies  $f$  and pathlengths  $p$  is shown in Fig. 2A-D.

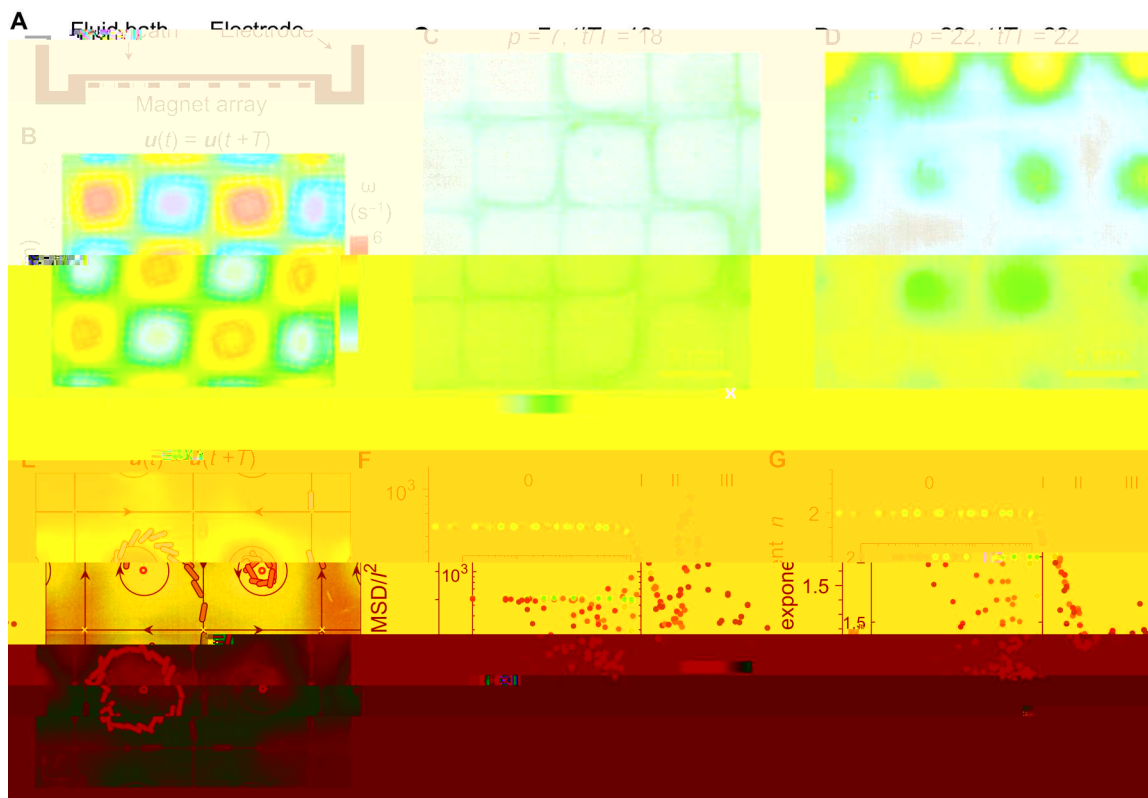


**Fig. 1. Dispersion patterns of active bacteria and long-term swimmer transport from the Langevin model reveal distinct dispersion regimes mediated by the time-periodic flow.** (A) Schematic of the periodic flow cell apparatus used in the experiments. (B) Flow vorticity and velocity vectors in the experimental flow cell, obtained by particle tracking velocimetry. (C and D) Cell distribution patterns in bacteria dispersion experiments using *V. cholerae* labeled with green fluorescent protein (GFP) at (C) pathlength  $p = 7$  and time  $t/T = 18$  in the manifold trafficking regime and (D) pathlength  $p = 20$  and time  $t/T = 2$  in the vortex trapping regime. Colors indicate GFP intensity, a.u., arbitrary units. (E) Schematic of active swimmer transport in the time-periodic flow. Black arrows indicate directions of vortices and flow manifolds, which connect hyperbolic fixed points (white crosses). Fluorescent bacterial swimmers (green) are allowed to disperse under time-periodic flow. As flow pathlength increases, a subset of swimmers spiral outward the initial vortex and participate in chaotic transport along flow manifolds (blue, regime II). At high pathlength, increasing numbers of swimmers are trapped (red, regime III) near elliptic points (red circles). Swimmer orientation is indicated by the angle  $\theta$ . (F) Ensemble-averaged stroboscopic MSDs of active swimmers as a function of flow pathlength  $p$  for various flow frequencies  $f$  and flow peak vorticities  $\omega$  at time  $t = 2000$  s, normalized by the flow quarter-cell length  $l^2$  for  $u_s = 80 \mu\text{m/s}$ . Inset: Identical MSD plotted against  $p$ . (G) The corresponding MSD scaling exponent  $n$ . Inset: Identical exponent  $n$  plotted against  $p$ . The designations 0, I, II, and III in (F) and (G) indicate transport regimes.

a various cases of the process for each of the scenarios described above. Before the onset of the epidemic (before  $t = 0$ ), we assume the SD based on the evaluation of the free-swimming case, we find a steady state (see Fig. 2, A and C, above S1); we show the evolution of the variables over time.

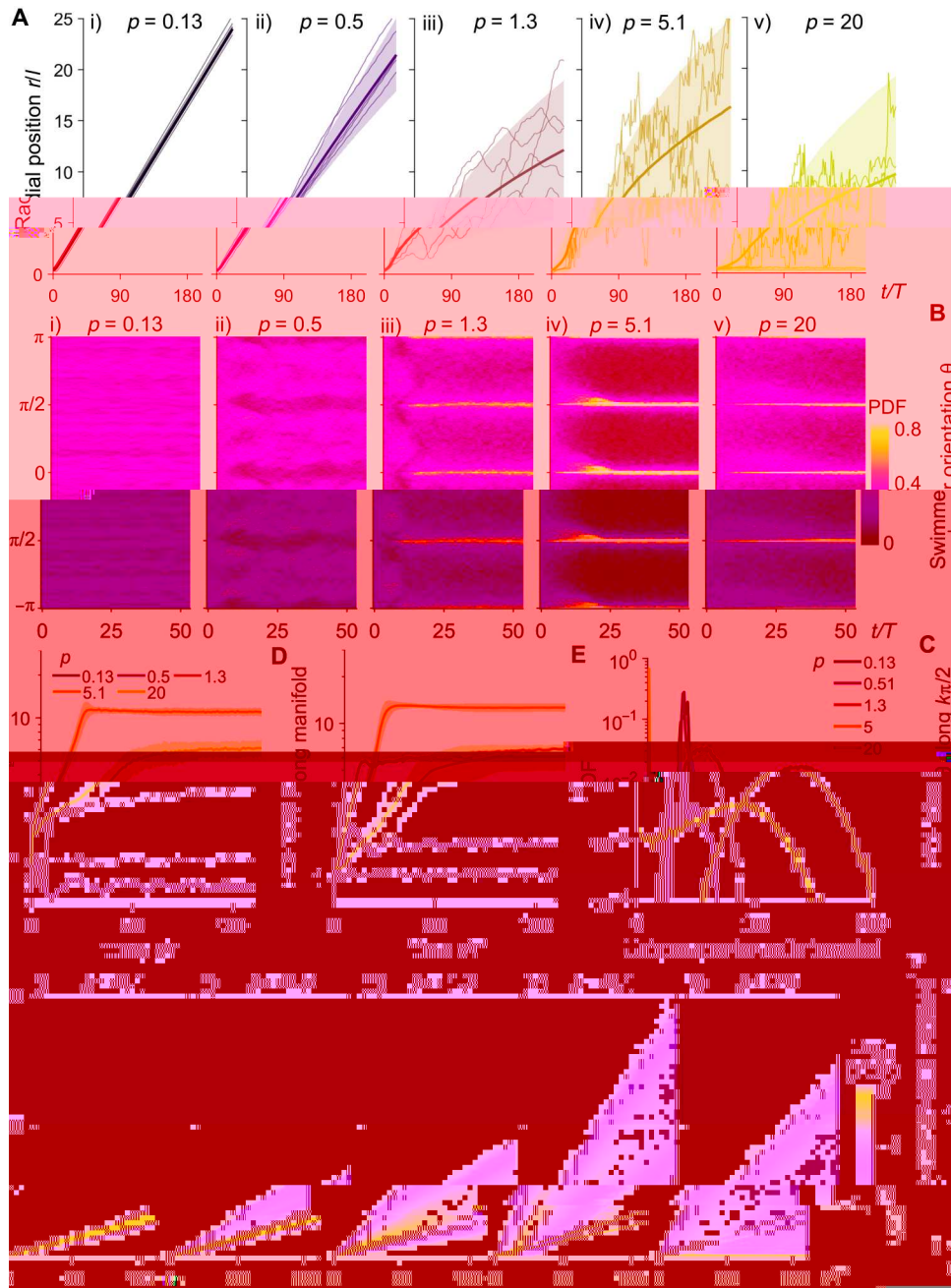


**Fig. 3. Swimmer radial spreading, swimming orientation bias, aggregation toward flow manifolds, and unique flow cells traveled are nonmonotonically controlled by the flow pathlength**

flow a fo s,  $F_{\nu, 3B}$ ). I e a fo affc  $\nu$  e  $p=5,1$ , e o a o a a s ace e ceases co a e o a a  $p=1,3$   $\nu, F_{\nu, 3A}$ ) acco a ce w e cease SD va es  $F_{\nu, 1B}$ ). T e v a sw e a eco es osc a e w a e a e s a s o e e sca e, a sw e a e e a o a fo s s ax  $\nu, F_{\nu, 3B}$ ). Las, e vo ex e ce o ce a  $\nu, F_{\nu, 3A}$ ). I v a sw e a eco es co e o ex b a e c a o c e v a o s fo e o a o e a, w e a s bse of sw e s beco e a e e a q a e -ce. T e a e a o a fo s s w e a e e co a e o a a  $p=5,1$   $\nu, F_{\nu, 3B}$ ).

To q a fy e evo o of sw e a e w fow a fo s, we co e e bas of obab y es y f co PDF) of  $\theta$  a o  $k\pi/2$  as af c o of  $p$  see  $F_{\nu, 3C}$  a a e as a e o s). T e bas s e f e as e PDF o a e by a of a a o fo s s b o. W e o o e a o a bas occ s e f ee-sw  $\nu$  e  $p=0,13$ ), we f w e a sw e e o fo a fo s a e o se of fow ce a s o; o e a e PDF bas fa s be ow 1 fo  $p=0,5$ . As e fow s e f e ceases o  $p=5,1$ , sw e s beco e ceas y a e w fow a fo s, eac a a o e of a e cease e obab y bas befo e a e y ceas a e ax  $p=20$ . Sw e a a o y a cs s ow s a e s  $F_{\nu, 3D}$ ). Sw e a a ces beco e ceas y a a e o wa fow a fo s as  $p$  ceases, eac a a o e of a e cease obab y a  $p=5,1$  befo e ceas a  $p=20$  e o a a e vo ex co e. Ove a, we f a e e e s c-o-c a o c a s o v a ce a eco es e e e fow ce e a ce e s a s o a e o a o eve. T e co ec ve co ve e ce o wa a a e w fow a fo s e abes bseq e c a o c affc a by e e e o c fow.

### An optimal dispersion regime occurs at intermediate pathlengths

Fow ce a s o ca f e ce e ab y of co o a s s o ex o e e fow o a a fo a e fo e s. T e ab y o co ve a e fow a o s o vo es) s co c ve o e access, w e eas a e s s a e e e e o. He e,

we q a fy s be av o by o o a e s a s cs of q e q a e -ce s ave e by e sw e s e s e s o as af c o of fow a e  $p$   $F_{\nu, 3E}$ ). I e f ee-sw  $\nu$  e  $p=0,13$ , e PDF s b o s ow s a a ow e a a o a s a se of q a e -ce s. T ese q a e -ce s o ca e a o e sw e a eco y, as s ow by e e a cease e be of q e q a e -ce s ave e w e  $\nu, F_{\nu, 3F}$ ). As fow ce a s o co e ces  $0,51 < p < 5$ ), e s b o of q e q a e -ce s ave e w e s a s fs o e va es  $F_{\nu, 3E}$ ). T s es ca es a sw e s a e ceas y ab e o ex o e a a e se of vo ex ce s as  $p$  ceases. I a o, e e eve o e of e s a s cs ceas y fo ows a sq a e o o e a o s  $\nu, F_{\nu, 3F}$ ), co s se w e ff s ve a e of e fow ce a s o. T se a ce e effec s ax  $p=5,1$  e a fo affc  $\nu$  e  $F_{\nu, 3, E}$  a  $F, \nu$ )

swimmers  $u_s T/l = 0.18 \pm 0.25$ ; Fig. 4B) show they are by a factor of  $\sim 2$  faster than the theoretical prediction. This increase is associated with a lower swimming speed in the presence of confinement, which is expected to be due to the hydrodynamic interactions between the swimmer and the walls.

### Swimming speed affects dispersion rate but not the patterns in the manifold confinement regime

For slow swimmers (quiescent flow  $v = 0$ ), we observe a decrease in the swimming speed as the confinement becomes stronger. Here, we explore the effects of confinement on the dispersion rate of a single swimmer. We consider a swimmer in a confined space, where the confinement is defined as the ratio of the swimming speed to the confinement length  $u_s T/l$  (Fig. 4C). For  $u_s T/l < 1$ , the dispersion rate is lower than in the unconfined case. This is because the swimmer's trajectory is more constrained by the walls, leading to a smaller displacement over time. For  $u_s T/l > 1$ , the dispersion rate is higher than in the unconfined case. This is because the swimmer's trajectory is more erratic due to the confinement, leading to a larger displacement over time. The transition between the two regimes occurs at  $u_s T/l \approx 1$ .

### Swimmers engage in chaotic escape spirals with exponential scaling in time before trafficking along manifolds

These escape spirals are observed when the swimming speed is high enough to overcome the confinement (Fig. 5). We find that the dispersion rate follows an exponential scaling with time, which is characteristic of chaotic behavior. This is observed when the swimming speed is high enough to overcome the confinement (Fig. 5). The transition between the two regimes occurs at  $u_s T/l \approx 1$ . For  $u_s T/l < 1$ , the dispersion rate is lower than in the unconfined case. This is because the swimmer's trajectory is more constrained by the walls, leading to a smaller displacement over time. For  $u_s T/l > 1$ , the dispersion rate is higher than in the unconfined case. This is because the swimmer's trajectory is more erratic due to the confinement, leading to a larger displacement over time. The transition between the two regimes occurs at  $u_s T/l \approx 1$ .

we observed a 10% increase in the swimming speed compared to the unconfined case (Fig. 5C).

We explore the effects of confinement on the dispersion rate of a single swimmer. We consider a swimmer in a confined space, where the confinement is defined as the ratio of the swimming speed to the confinement length  $u_s T/l$  (Fig. 5B). For  $u_s T/l < 1$ , the dispersion rate is lower than in the unconfined case. This is because the swimmer's trajectory is more constrained by the walls, leading to a smaller displacement over time. For  $u_s T/l > 1$ , the dispersion rate is higher than in the unconfined case. This is because the swimmer's trajectory is more erratic due to the confinement, leading to a larger displacement over time. The transition between the two regimes occurs at  $u_s T/l \approx 1$ .

The transition between the two regimes occurs at  $u_s T/l \approx 1$ . For  $u_s T/l < 1$ , the dispersion rate is lower than in the unconfined case. This is because the swimmer's trajectory is more constrained by the walls, leading to a smaller displacement over time. For  $u_s T/l > 1$ , the dispersion rate is higher than in the unconfined case. This is because the swimmer's trajectory is more erratic due to the confinement, leading to a larger displacement over time. The transition between the two regimes occurs at  $u_s T/l \approx 1$ .

### Faster swimming facilitates escape from chaotic limit cycles in the vortex trapping regime

To probe the effects of confinement on the dispersion rate, we consider a swimmer in a confined space. We find that the dispersion rate follows an exponential scaling with time, which is characteristic of chaotic behavior. This is observed when the swimming speed is high enough to overcome the confinement (Fig. 5). The transition between the two regimes occurs at  $u_s T/l \approx 1$ .

Downloaded from https://www.science.org on December 09, 2022

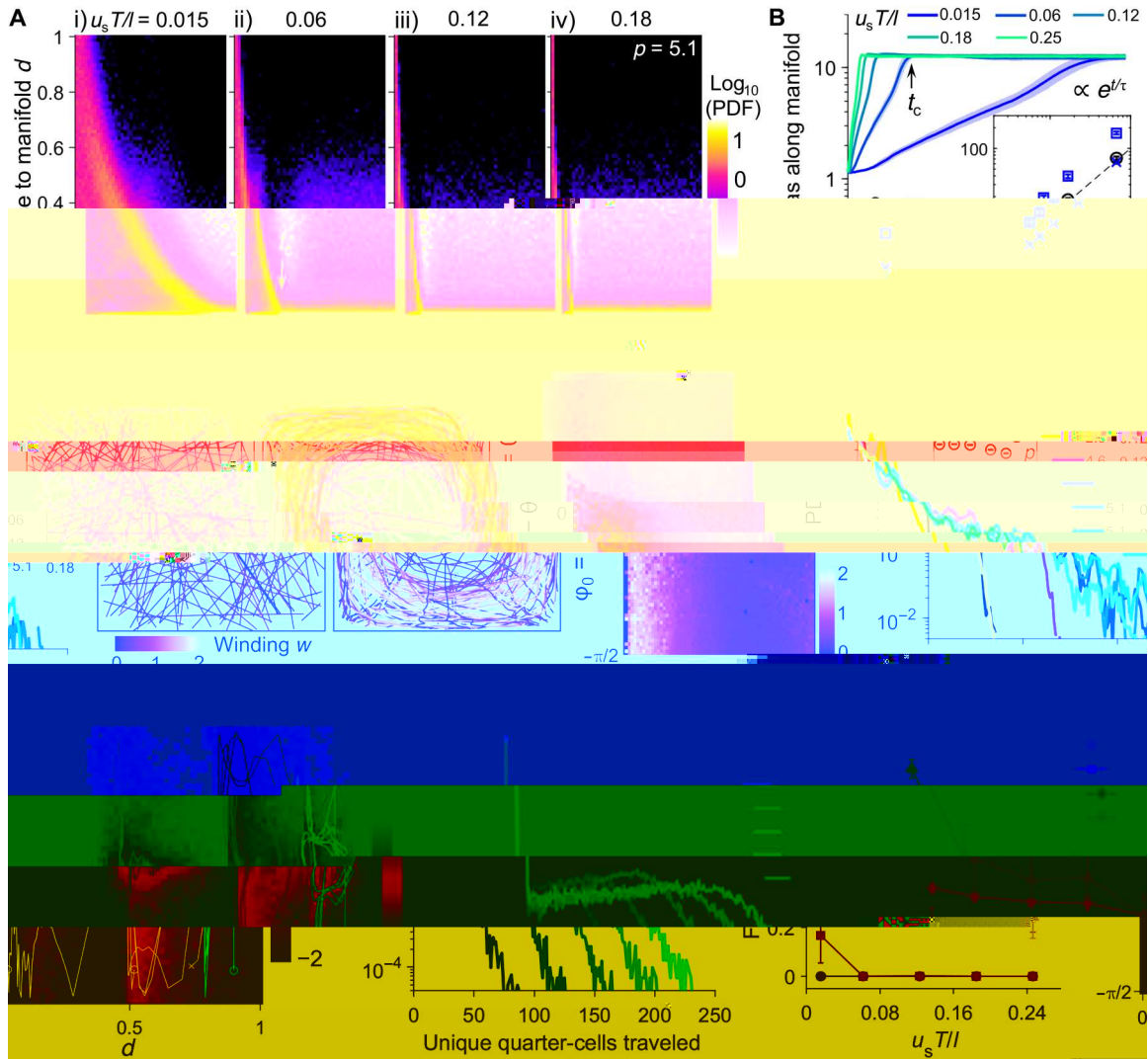


**Fig. 5. Effect of swimming speed on transport dynamics in the manifold trafficking and vortex trapping regimes.** (A) PDF distribution of swimmer distance to flow manifolds  $d$ , in the manifold trafficking regime  $p = 5.1$ , for (i)  $u_s T/l = 0.015$ , (ii)  $u_s T/l = 0.06$ , (iii)  $u_s T/l = 0.12$ , and (iv)  $u_s T/l = 0.18$ . White arrow indicates the critical time  $t_c$  to reach flow manifolds. (B) PDF bias of swimmer aggregation toward flow manifolds for various values of  $u_s T/l$ . Black arrow indicates the critical time  $t_c$  of the exponential growth, the critical time  $t_c/T$ , and the critical time of arrival without flow  $t_c/T$  a.n.f., versus inverse scaled swimming speed  $l/u_s T$ . Dashed line: The abscissa is equal to the ordinate. (C and D) Swimmer trajectories before reaching flow manifolds  $u_s T/l = 0.12$  for (C)  $p = 0.13$  and (D)  $p = 5.1$ . Colors indicate trajectory winding  $w$ . (E) Population-averaged winding  $\langle w \rangle$  before reaching flow manifolds, in the space of swimmer initial distances to flow manifolds,  $d_0$ , and orientations relative to the manifolds,  $\phi_0$ .

sea (es) for ex e es, T ese sw es say w e  
 c ao c sa w o e e a e a s o b a e s a c a  
 d va es) o e b o e a o s. Howe v, occas o a y, ese  
 sw es e o a e exc o s s d a e va o s fo a e  
 e w e fow. T e c a o c s o b o s c o s w e a e c o e s  
 e  $(X, y)$  s a c e a e s o w f, S10. We o e a sw es a  
 a e a y e a fow a fo s a a e s w e a way fo e  
 e c o o o e a e. T e y o e e e s a c a e e  
 fow-e a b e a f f c a a e x o e a a e e b e of fow  
 ce s  $F_q$ , 5H),

Las, fas e sw es ave s a f c a a s o a va a e s o v e  
 s o w sw es e v o e x a e e, F s, a c e a s e  
 sw e s e e a  $p = 20$  e s s a a e b e of fow ce s  
 ave e  $F_q$ , 5H) w e e e o a o - e v e s e s o  $\langle n_q \rangle$  s c a e s  
 w e s q a e o o of e sw e s e e  $F_q$ , 5H, se),  
 Seco, fas e sw es a e a s o b e e a e s c a e v o e x a e  
 a s o w e s w es  $F_q$ , 5I), P a s e a a s fo e fow-  
 ce sw e a s o a a a a s f c o s of b o  
 sw e s e e a fow a e a e s a e f, S11,  
 He ce, e s o e s e e e o c fow, sw es a e o c e



eratic sea of fow a fo sa ob  
c ao c cycles, Fas e sw es, oweve, ca esca efow  
ce a a co e o ex o e efow o a ,

**DISCUSSION**

coo a s of e e co e sea y fows bo a ea  
s a a ca o s, T e co a be wee o ya fow s  
c ca o e s e s o , e o c o , a ove a s v va of  
c o s w e s, I o c e a s, i ve s, a b o e a c o s, s e a y f o w s  
w s o o c a v e o c y a e s a e e s e a c o s s a a e  
a e of e s c a e s a e s c a e s, W e s w e r a s o  
a s b e e x e s v e y s e s e a y f o w s o f v o e x a c o v e c  
o o a r a y s, e e, w e e x o e e c a o c a o o o o c  
a s o f c o s w e s v a a o e e e o c x  
f o w s a b o L a e v s a o s a b a c e a s e s o e x  
e e s, T w o o e s o a a a e e s c o o e a c v e  
s w e s a s o e s e a y f o w, a e y, e a e e ,  
w c s e s e a e o f e b a c o f o w, a o e s o a  
s w e s e e a v e o e f o w, F o f x e - s e e s w e s  
w e a B o w a e f f e c s, c e a s e a e a a e  
e e v e a e e e s c f o w - e a b e a s o a e s w  
o a b y f f e e s e s o y a c s, A o e a e f o w s e  
e a v e o s w e s, e s w e s a e c e a s y a a c e  
o w a e b o a e s o f e f o w c e s, e a o a a e e c  
o SD a s o w e a e o f b a s c s w e s, A s a  
e f e c e a s e s, a s c f o w - c e a s o e e e s  
a a y s e s e s w e s a c a o c a e y f f s v e  
f a s o a o a s f o e b y v o e x b o a e s, T o a c a e  
e c a o c a f f c a o v o e x b o a e s, o w e v e, a  
s b s e o f s w e s e o e s c a e e v o e v a e a o e a  
s a s a a e v e s a f o s w e s, f a s o s o w, F a c a e b y  
e c a o c a s o a o f o w a f o s, e b e o f q e  
f o w c e s a v e s e b y s w e s e s e s o s a x e ,  
e a o e a e s e x o s e o o e a f o a o s  
e f o w o a, S c e a c e e s o o e x e e f e y,  
o w e v e, a s f e c e a s e s f o w s e e s e f a e  
o f s w e s o e s c a e e v o e x, I s e a, s w e s a e o c e  
c a o c c y c e s w e v o e x, T e o a s e s o  
e e e s e o e c o e o b e w e e c a o c a s o a  
e v o e x b o a e s a e s o e o e a o a a a  
a e v o e x c o e, F a s e s w e s e s s v e y o v e c o e f o w  
e a a a e f f e c e s e s o s f o w  
e, O e s s o w a, a o e s w e s s a c e e  
e o f o w a o e s f y e v e s e a y v e c y c e, e e o c  
f o w s c a s f a e a y a e e a s o o c o e a s  
e s o o f e s w e v a e o e a a c a o c c o  
b e w e e f o w e s c a e, v e o c y, a s w e o y,

T e w o o e s o a c o o a a e e s a y b e e e a  
b e y o e s e c f c s o f e f o w s y s e e e o e s c o e a c v e  
a e a s o s e a y f o w s f o s o o s w e s w a  
a e o f s a e s, s e e s, a o a o a f f s v e s, O e s s  
w b e e s e c a y e e v a f o s y e c a c v e c o o s s c a s  
a s e a e c e s a c e e o a o a f f s v y, f a s  
s w e s w e o a o a e o e a o s w e a c o a e o b a  
s c s w e s, a b a c e a s e c e s a o o a a b e,  
s c a s s o o - s w e s *Bacillus subtilis* a c e o a x s a s  
s c a s  $\Delta cheY$  a s f o *Escherichia coli* a  $\Delta cheY3$  a s  
*V. cholerae* 43),

We o e s e v e a a o s f o e c e e s y, W e o o c o  
s e s w e s w f e q e e o e a o s, S e c o, o o e  
e a s s w e s a s o a c e s a o o o c a y o f y e  
o s e f o w, T e f o e, w e c a o a c c a e y c a e e a s o  
b e a v o f e x e e y e s e c o b a s s e s o s, w e e s e c  
e a c o s, f e s e e f f e c, a f e e b a c o e f o w a e o  
o c e, I a o s o f s a v e o c y a e, s c a s y e b o c  
o s a f o w a f o s, a s a v a a o s w e s o s o  
e o e c o e a o s b s a a v a a o s s w e a  
e c o y, L a s, e x e e a y o b a e e s o o o e  
SD a SD s c a e x o e s f o c o e e - s e b a c e a  
o v e c e e e - s e f o w c e s, e s e c a y e s o o  
f o w a e s, e e s e s a s b s a a c a e e, w c w e s e  
o a e s s f e w o s,

W e y o e s e a c o f e e a f o w a f o s a o e a e  
f o w s a a e v o e x c o e s a s o f o w s f o e e e  
e s a y e a o c e a s w e e c o e a e s, e e e  
e a e s e s a c e o a a c e s, a o c a a c c  
a o f q o e s e s a a o e c e s a a s e s, A  
e a o s e s e b o c a s e e e b y e e e o c  
f o w a y a v e s f c a c a o s c a a s o s  
c o b a f e s y e a s v v a s a e s, F o w - c e s e s o  
s o s e v e f o s o w s w e s c o a e o f e e s w e  
q e s c e f o w, H e c e, b y c a e f s e e c o a c o o f f o w s c  
e a a e e, o e c a e v s e a o a a s o s a a y o  
a x e c o b e s e s o e e o c f o w s y s e s s c a s  
x b o e a c o s, e s e c a y f o s w e s w e o y,  
F e e o e, b y e x o e v o e x a e e a a  
e e, w e e f a s e s w e s e s c a e e a f o w c e c  
q c e a s o w s w e s, o e c o e s a b e e v c e s o  
e f e a y s o s w e s b y s e e, O e s s o e o e a  
c o a b e w e e f o w s c e, e e o c y, a s w e  
a s o c o a s o a v e c a o s f o e f e s y e a s o s  
a a f a e s o s a a e o a s s,

**MATERIALS AND METHODS**

**Langevin simulation**

A e e o c 2D T a y o - G e e v o e x y e o f f o w s s e e  
L a e v s a o, I e X, y) a e, e s e a f c o  $\psi$  o f e  
f o w s

$$\psi = \frac{UL}{2\pi} \cos(2\pi ft) \cos(2\pi x - L) \cos(2\pi y - L) \tag{1}$$

w e e U s e e a f o w v e o c y a f o w a f o s, f s e f e q e c y  
o f e f o w, L = 2l s e w a v e e o f e e o c f o w c e a  
c o s s o f f o q a e - c e s, a l = 6,5 s e w o f e  
q a e - c e, T e e a v o c y a v o e x c o e s s = 2\pi U/l, T e v e  
o c y f e s e  $u = \langle \psi_y - \psi_x \rangle$ , w e e X, y s b s c e o e  
a a f f e e a o, I a o, w e f e a o e s o a  
f o w a e a a e e p = UT/2\pi l = /4\pi^2 f, w c s e  
o a a e s w e b y e f o w e a e v o e x c o e a c y c e,  
o a e b y a f c e e, T e o e s o a a e s a  
e e a f e a o f e e o c f o w,

W e o e e s w e s a s a c v e e s o s o v a o e  
a o a x s 31, 47), w o s e o e a o a e w + x a x s s v e b y  
 $\theta$ , T e a s e c a o o f e s w e s  $\gamma \gamma = 5$  f o *V. cholerae* e s s  
o e w s e s a e ) a e o e y a a e e =  $\gamma^2 - 1 / \gamma^2 + 1$ ,  
T e s w e s e e s  $u_s, u_s = 80 \mu$  / s f o *V. cholerae* e s s

Downloaded from https://www.science.org on December 09, 2022

of the swimmer's velocity by the flow velocity  $\mathbf{u}$  and the swimming velocity  $\mathbf{u}_s$ .

$$d\mathbf{q} = \left[ \frac{\nabla\mathbf{u} - \nabla\mathbf{u}^T}{2} + \alpha \frac{\nabla\mathbf{u} + \nabla\mathbf{u}^T}{2} \cdot (\mathbf{I} - \mathbf{q} \otimes \mathbf{q}) \right] \mathbf{q} dt \quad (2a)$$

$$d\mathbf{x} = (\mathbf{u} + u_s \mathbf{q}) dt + \sigma_s d\mathbf{W} \quad (2b)$$

where  $\mathbf{q}$  is the swimmer's orientation,  $\mathbf{x} = (x, y)$  is the position vector of the swimmer,  $\nabla\mathbf{u}$  is the flow velocity gradient,  $\mathbf{W} = (W_x, W_y)$  is the Wiener process,  $W_x, W_y$  are independent Wiener processes with variance  $\sigma_s^2$ . We consider a two-dimensional flow  $\mathbf{u} = (u_x, u_y)$  in the  $x, y$  plane. The velocity field is assumed to be Gaussian with zero mean and covariance matrix  $D_0 = \sigma_s^2 n_s$ , where  $n_s = 2$  is the dimension of the system. The swimmer's position is given by the Stratonovich equation  $d\mathbf{x} = (\mathbf{u} + u_s \mathbf{q}) dt + \sigma_s d\mathbf{W}$ . The swimmer's orientation is given by the equation  $d\mathbf{q} = \left[ \frac{\nabla\mathbf{u} - \nabla\mathbf{u}^T}{2} + \alpha \frac{\nabla\mathbf{u} + \nabla\mathbf{u}^T}{2} \cdot (\mathbf{I} - \mathbf{q} \otimes \mathbf{q}) \right] \mathbf{q} dt$ . The swimmer's position is given by  $d\mathbf{x} = (\mathbf{u} + u_s \mathbf{q}) dt + \sigma_s d\mathbf{W}$ . The swimmer's orientation is given by  $d\mathbf{q} = \left[ \frac{\nabla\mathbf{u} - \nabla\mathbf{u}^T}{2} + \alpha \frac{\nabla\mathbf{u} + \nabla\mathbf{u}^T}{2} \cdot (\mathbf{I} - \mathbf{q} \otimes \mathbf{q}) \right] \mathbf{q} dt$ .

$$d\theta = \left[ -\frac{\psi_{xx} + \psi_{yy}}{2} + \alpha \left( \frac{\psi_{yy} - \psi_{xx}}{2} \cos 2\theta - \psi_{xy} \sin 2\theta \right) \right] dt + \sigma dW_\theta \quad (3a)$$

$$dx = (\psi_y + u_s \cos \theta) dt + \sigma_s dW_x \quad (3b)$$

$$dy = (-\psi_x + u_s \sin \theta) dt + \sigma_s dW_y \quad (3c)$$

The area of the swimmer's path is  $A = \int dx dy$ . For each realization of the flow coordinates,  $10^4$  swimmers are simulated. The swimmer's position is given by  $d\mathbf{x} = (\mathbf{u} + u_s \mathbf{q}) dt + \sigma_s d\mathbf{W}$ . The swimmer's orientation is given by  $d\mathbf{q} = \left[ \frac{\nabla\mathbf{u} - \nabla\mathbf{u}^T}{2} + \alpha \frac{\nabla\mathbf{u} + \nabla\mathbf{u}^T}{2} \cdot (\mathbf{I} - \mathbf{q} \otimes \mathbf{q}) \right] \mathbf{q} dt$ . The swimmer's position is given by  $d\mathbf{x} = (\mathbf{u} + u_s \mathbf{q}) dt + \sigma_s d\mathbf{W}$ . The swimmer's orientation is given by  $d\mathbf{q} = \left[ \frac{\nabla\mathbf{u} - \nabla\mathbf{u}^T}{2} + \alpha \frac{\nabla\mathbf{u} + \nabla\mathbf{u}^T}{2} \cdot (\mathbf{I} - \mathbf{q} \otimes \mathbf{q}) \right] \mathbf{q} dt$ .

By setting  $x = x/l$ ,  $y = y/l$ ,  $t = t/T$ ,  $\psi = \psi T^2/l^2$ ,  $u_s = u_s T/l$ , and  $\sigma_s = \sigma_s/l$ , the above equation can be written as

$$\dot{\psi} = 2p \cos(2\pi t) \cos(\pi x) \cos(\pi y) \quad (4a)$$

$$d\theta = \left[ -\frac{\psi_{xx} + \psi_{yy}}{2} + \alpha \left( \frac{\psi_{yy} - \psi_{xx}}{2} \cos 2\theta - \psi_{xy} \sin 2\theta \right) \right] dt + \sigma dW_\theta \quad (4b)$$

$$dx = (\psi_y + u_s \cos \theta) dt + \sigma_s dW_x \quad (4c)$$

$$dy = (-\psi_x + u_s \sin \theta) dt + \sigma_s dW_y \quad (4d)$$

where  $p$  is the strength of the flow,  $u_s$  is the swimming velocity,  $\psi$  is the velocity field,  $\sigma_s$  is the diffusion coefficient, and  $\sigma$  is the noise strength. The swimmer's position is given by  $d\mathbf{x} = (\mathbf{u} + u_s \mathbf{q}) dt + \sigma_s d\mathbf{W}$ . The swimmer's orientation is given by  $d\mathbf{q} = \left[ \frac{\nabla\mathbf{u} - \nabla\mathbf{u}^T}{2} + \alpha \frac{\nabla\mathbf{u} + \nabla\mathbf{u}^T}{2} \cdot (\mathbf{I} - \mathbf{q} \otimes \mathbf{q}) \right] \mathbf{q} dt$ .

### Swimmer statistics

Let us consider the swimmer's statistics. The swimmer's position is given by  $d\mathbf{x} = (\mathbf{u} + u_s \mathbf{q}) dt + \sigma_s d\mathbf{W}$ . The swimmer's orientation is given by  $d\mathbf{q} = \left[ \frac{\nabla\mathbf{u} - \nabla\mathbf{u}^T}{2} + \alpha \frac{\nabla\mathbf{u} + \nabla\mathbf{u}^T}{2} \cdot (\mathbf{I} - \mathbf{q} \otimes \mathbf{q}) \right] \mathbf{q} dt$ . The swimmer's position is given by  $d\mathbf{x} = (\mathbf{u} + u_s \mathbf{q}) dt + \sigma_s d\mathbf{W}$ . The swimmer's orientation is given by  $d\mathbf{q} = \left[ \frac{\nabla\mathbf{u} - \nabla\mathbf{u}^T}{2} + \alpha \frac{\nabla\mathbf{u} + \nabla\mathbf{u}^T}{2} \cdot (\mathbf{I} - \mathbf{q} \otimes \mathbf{q}) \right] \mathbf{q} dt$ .

### Bacterial strain and suspension preparation

We used the *V. cholerae* strain C6706 (LZV918) as the bacterial strain. The *V. cholerae* strain C6706 (LZV918) is a non-toxigenic strain. The bacterial suspension was prepared by growing the bacteria in LB medium at 37°C for 24 hours. The bacterial concentration was adjusted to  $1 \times 10^8$  cells/ml. The bacterial suspension was used for the flow cell experiments.

### Flow cell apparatus

The flow cell apparatus consists of a glass channel of length  $100 \mu\text{m}$  and width  $10 \mu\text{m}$ . The flow cell is filled with the bacterial suspension. The flow cell is connected to a syringe pump. The flow rate is controlled by the syringe pump.

The Stokes number,  $St$ , is defined as the ratio of the particle relaxation time to the characteristic time of the flow. For a spherical particle of diameter  $d_p$  and density  $\rho_p$  in a fluid of viscosity  $\mu$  and density  $\rho_f$ , the relaxation time is  $\tau_r = \frac{d_p^2 \rho_p}{18\mu}$ . The characteristic time of the flow is  $\tau_f = \frac{L}{U}$ , where  $L$  is the characteristic length scale and  $U$  is the characteristic velocity. The Stokes number is then  $St = \frac{\tau_f}{\tau_r} = \frac{\rho_f U L}{\rho_p d_p^2}$ .

### Bacterial dispersion experiments

In a series of experiments, the dispersion of bacteria in a flow was studied. The flow was generated in a pipe of diameter  $D = 50$  mm. The bacteria were introduced at the inlet of the pipe. The flow velocity was  $U = 0.02$  to  $2$  m/s. The Reynolds number of the flow, defined by  $Re = \frac{UD}{\nu}$ , based on the kinematic viscosity  $\nu$ , varied from  $0.1$  to  $10$ . The Peclet number, defined by  $Pe = \frac{UD_0}{D_0}$ , where  $D_0$  is the diffusion coefficient, varied from  $10^5$  to  $10^7$ . The experiments were conducted in a Taylor-Couette geometry. The results showed that the dispersion of bacteria was significantly affected by the flow velocity and the Reynolds number.

### Particle tracking velocimetry

To characterize the flow, particle tracking velocimetry (PTV) was used. The particles were seeded in the flow at a concentration of  $10^4$  to  $10^5$  particles per cubic centimeter. The particles were tracked using a high-speed camera. The camera was positioned at a distance of  $180$  mm from the flow. The flow velocity was  $U = 0.02$  to  $2$  m/s. The PTV results showed that the flow was highly turbulent. The velocity fluctuations were on the order of  $10\%$  of the mean velocity. The PTV results also showed that the particles were dispersed throughout the flow.

The results of the PTV experiments are shown in Figure 1. The figure shows the velocity field of the flow. The velocity is color-coded, with red representing the highest velocity and blue representing the lowest velocity. The flow is highly turbulent, with large velocity fluctuations.

34. N. Khurana, N. T. Ouellette, Interactions between active particles and dynamical structures in chaotic flow. *Phys. Fluids* **24**, 091902 (2012).
35. Y. Li, Y. Zhou, F. Marchesoni, P. K. Ghosh, Colloidal clustering and diffusion in a convection cell array. *Soft Matter* **18**, 4778–4785 (2022).
36. Q. Yin, Y. Li, B. Li, F. Marchesoni, S. Nayak, P. K. Ghosh, Diffusion transients in convection rolls. *J. Fluid Mech.* **912**, A14 (2021).
37. T. Bhattacharjee, S. S. Datta, Bacterial hopping and trapping in porous media. *Nat. Commun.* **10**, 2075 (2019).
38. C. Kurzthaler, S. Mandal, T. Bhattacharjee, H. Löwen, S. S. Datta, H. A. Stone, A geometric criterion for the optimal spreading of active polymers in porous media. *Nat. Commun.* **12**, 7088 (2021).
39. A. Dehkharghani, N. Waisbord, J. Dunkel, J. S. Guasto, Bacterial scattering in microfluidic crystal flows reveals giant active Taylor–Aris dispersion. *Proc. Natl. Acad. Sci. U.S.A.* **116**, 11119–11124 (2019).
40. G. A. Voth, G. Haller, J. P. Gollub, Experimental measurements of stretching fields in fluid mixing. *Phys. Rev. Lett.* **88**, 254501 (2002).
41. P. E. Arratia, J. P. Gollub, Statistics of stretching fields in experimental fluid flows exhibiting chaotic advection. *J. Stat. Phys.* **121**, 805–822 (2005).
42. G. B. Jeffery, L. N. G. Filon, The motion of ellipsoidal particles immersed in a viscous fluid. *Proc. R. Soc. A* **102**, 161–179 (1922).
43. D. S. Bischoff, G. W. Ordal, *Bacillus subtilis* chemotaxis: A deviation from the *Escherichia coli* paradigm. *Mol. Microbiol.* **6**, 23–28 (1992).
44. J. R. Howse, R. A. L. Jones, A. J. Ryan, T. Gough, R. Vafabakhsh, R. Golestanian, Self-motile colloidal particles: From directed propulsion to random walk. *Phys. Rev. Lett.* **99**, 048102 (2007).
45. M. Shigematsu, Y. Meno, H. Misumi, K. Amako, The measurement of swimming velocity of *Vibrio cholerae* and *Pseudomonas aeruginosa* using the video tracking methods. *Microbiol. Immunol.* **39**, 741–744 (1995).
46. S. Kojima, K. Yamamoto, I. Kawagishi, M. Homma, The polar flagellar motor of *Vibrio cholerae* is driven by an Na<sup>+</sup> motive force. *J. Bacteriol.* **181**, 1927–1930 (1999).
47. W. M. Durham, E. Climent, R. Stocker, Gyrotaxis in a steady vortical flow. *Phys. Rev. Lett.* **106**, 238102 (2011).
48. J. C. Crocker, D. G. Grier, Methods of digital video microscopy for colloidal studies. *J. Colloid. Interf. Sci.* **179**, 298–310 (1996).

**Acknowledgments:** We acknowledge H. A. Stone and B. L. Bassler for insightful discussions and feedback to the manuscript. We thank the members of the Arratia and Bassler research groups for insightful discussions and R. Winter and M. Gurjar for help with early work. **Funding:** This work was supported by NSF-DMR-1709763. B.Q. holds a Career Award at the Scientific Interface from the Burroughs Wellcome Fund. **Author contributions:** B.Q. and P.E.A. designed the research; B.Q. performed experiments and simulations; B.Q. and P.E.A. analyzed data; and B.Q. and P.E.A. wrote the paper. **Competing interests:** The authors declare that they have no competing interests. **Data and materials availability:** All data needed to evaluate the conclusions in the paper are present in the paper and/or the Supplementary Materials.

Submitted 23 June 2022  
Accepted 1 November 2022  
Published 7 December 2022  
10.1126/sciadv.add6196

## Confinement, chaotic transport, and trapping of active swimmers in time-periodic flows

Boyang QinPaulo E. Arratia

*Sci. Adv.*, 8 (49), eadd6196. • DOI: 10.1126/sciadv.add6196

### View the article online

<https://www.science.org/doi/10.1126/sciadv.add6196>

### Permissions

<https://www.science.org/help/reprints-and-permissions>

Use of this article is subject to the [Terms of service](#)